



An experimental and simulation study on the cold start behaviour of particulate filters with wall integrated three way catalyst

B. Opitz ^{a,b}, A. Drochner ^b, H. Vogel ^b, M. Votsmeier ^{a,*}

^a Umicore AG & Co. KG, Rodenbacher Chaussee 4, 63457 Hanau, Germany

^b Ernst-Berl Institut, Technische Universität Darmstadt, Petersenstr. 20, 64287 Darmstadt, Germany



ARTICLE INFO

Article history:

Received 18 March 2013

Received in revised form 24 June 2013

Accepted 27 June 2013

Available online 10 July 2013

Keywords:

Exhaust

GPF

Chemical reactors

Simulation

Light-off

Wall-flow

ABSTRACT

Upcoming legislation will most likely require the introduction of particulate filters for gasoline engines. One attractive technical solution combines the three way catalytic functionality and the filter in one device, the so called 'catalysed Gasoline Particulate Filter'.

The current study uses temperature step experiments and CO oxidation as a test reaction to compare the catalysed particulate filter and the conventional flow-through monolith with respect to their dynamic cold-start behaviour. Despite the fact that the two reactor configurations are tested with identical wash-coat formulation, precious metal loading and thermal mass, experiments show a significantly delayed cold-start for the particulate filter. The resulting cumulated CO emissions of the catalysed filter exceed those of the open monolith by 190–300% in the temperature range between 250 °C and 325 °C.

The experimental results are analysed by means of numerical simulation. In a first step a kinetic model of the CO oxidation is parameterised using only experimental data obtained for the conventional flow-through catalyst. The resulting kinetics are implemented in a model of the wall-flow filter. Without further modification of the kinetic parameters, this model quantitatively predicts the cold-start behaviour of the catalysed filter.

Finally, the numerical model is used in a sensitivity analysis to identify and quantify the individual physical effects contributing to the experimentally observed difference in the light-off behaviour. It is shown that a part of the observed difference in the cold-start performance can be traced back to differences in cell density and the heat capacity of the plugs. Even at identical cell density and without the plug effect the filter shows significantly higher CO emissions. It is shown that this intrinsic difference between the filter and the conventional monolith can be quantitatively explained by differences in heat transfer, internal mass transfer and external mass transfer.

© 2013 Elsevier B.V. All rights reserved.

1. Introduction

Gasoline particulate filters Today, Diesel Particulate Filters (DPFs) are standard emission control devices for diesel engines. Recently particulate filters are also considered for gasoline engines. Although the soot mass emitted by gasoline engines is orders of magnitude lower, particulate numbers can be high due to a lower average particle size [1]. Small particles are known to be more hazardous since they have a higher potential to penetrate the fine capillaries in the lung [2,3]. For this reason, upcoming legislation will also impose limits for the particulate number emissions of gasoline vehicles. Most likely this EURO 6 legislation will require the implementation of filter devices for gasoline engines [4]. This is especially evident for fuel efficient gasoline direct injection (GDI)

engines. These engines emit particle numbers that are an order of magnitude higher than those of conventional port fuel injected engines and can even exceed the particulate number emissions of diesel engines without DPF [5].

Probably the most economical way to remove soot from gasoline exhaust is to combine a conventional three way catalyst (TWC) and a particulate filter in one single device, the so called 'catalysed Gasoline Particulate Filter' (cGPF). This device consists of a ceramic filter with a three way washcoat finely dispersed inside the wall pore system. The cGPF is also referred to as a 'Four-Way Catalyst' since it simultaneously removes the four pollutants CO, hydrocarbons (HC), NO and soot.

The feasibility of the cGPF concept has recently been demonstrated in a number of studies [6–8]. Thereby it has been shown that the filtration efficiency of such systems is sufficient to fulfil the currently discussed particulate number limits, despite the small size of gasoline soot particles. Furthermore, the backpressure of the cGPF can be reduced to a level where the impact on fuel efficiency and CO₂ emissions becomes negligible [7,8].

* Corresponding author.

E-mail address: martin.votsmeier@eu.uminco.com (M. Votsmeier).

Besides filtration efficiency and backpressure, the development criteria for a cGPF are the same as for a conventional three way catalyst:

- CO and HC emissions, which are mainly influenced by the cold-start performance of the catalyst.
- NO emissions that are mainly caused by the interaction of the catalyst and a non-perfect lambda control system.

This paper focuses on the cold-start behaviour of the cGPF. Despite the fact that modern engines reach exhaust temperatures of several hundred degrees Celsius within a few seconds, cold-start is responsible for a significant part of total CO and hydrocarbon emissions. Due to the fast heat-up of the exhaust gas, the cold-start of the three way catalyst can be described as a dynamic light-off which is also called 'fast light-off'. This means that the temperature increase of the exhaust gas is fast compared to the characteristic time of the catalyst heat-up. Therefore, during cold-start a temperature front is moving through the catalyst from the inlet towards the outlet. This 'fast light-off' scenario is significantly different from the conventional stationary laboratory light-off test with a slow heating ramp, which leads to a more or less uniform temperature distribution within the entire catalyst.

In this paper we study the dynamic light-off performance of three way catalysts and cGPFs by temperature jump laboratory experiments. These experiments reproduce the dynamic light-off conditions of real vehicle operation in an idealised form with a simplified exhaust that contains CO as the only pollutant. The objective of the study is to compare the light-off performance of the catalysed filter to the performance of a conventional open monolith. It is shown that at constant washcoat loading, precious metal loading and thermal mass, the cGPF shows significantly higher cumulated CO emissions than the conventional open channel three way catalyst. In a second step a numerical model of the cGPF is presented and it is demonstrated that the higher emissions of the cGPF are nearly quantitatively predicted by the model. Finally, the model is used in a sensitivity analysis to gain an understanding of the physical effects that are responsible for the inferior light-off performance of the catalysed filter.

2. Open flow-through monolith versus wall-flow filter

The ceramic filter substrate is derived from an open flow-through monolith by plugging alternating channels at the inlet and the outlet so that the gas is forced to flow through the wall. In a conventional flow-through monolith the catalyst is applied as a thin layer on the channel walls while in a cGPF the catalyst is dispersed inside the porous wall. From a reaction engineering point of view, fundamental differences exist between the two reactor configurations. The flow-through monolith relies on diffusion for the transport of reactants and products between the catalytically active washcoat and the gas phase. In the wall-flow filter the reactants are forced through the catalytically active wall by convection. This situation was analysed by numerical flow simulations in [9]. Under steady state conditions the wall-flow filter showed higher conversion rates compared to the flow-through monolith. This was explained by the absence of mass transfer limitations in the case of the wall-flow filter. A more detailed analysis of the complex interplay of diffusion, convection and reaction in the wall flow reactor has been provided in [10]. It was shown that for the wall-flow filter operation two limiting cases can be distinguished:

- At low reaction rates and low flow velocities mass transfer in radial direction is entirely dominated by diffusion. This means that radial concentration gradients between the inlet and outlet

channel and inside the porous wall are negligible. The main concentration gradient is oriented in axial direction, just as in the case of the flow-through monolith.

- If reaction rates are high, radial transport is dominated by convection. In this case axial gradients along the channels become negligible and the main gradient is oriented in radial direction through the filter wall.

Under most operating conditions relevant for an automotive exhaust catalyst the filter is operated in an intermediate range where diffusion and convection both contribute to radial transport.

A model based analysis of the differences between the flow-through and wall-flow reactor concept has also been presented by Dardiotis et al. [11]. In this study the gas flow in the inlet and outlet channels is treated as one dimensional. Diffusive mass transfer is taken into account by mass transfer coefficients. The study confirms the conclusion that under steady state operation the wall-flow filter is expected to show higher conversion in those situations where the conventional flow-through monolith becomes mass transfer limited (short residence times, high reaction rates). In the context of diesel exhaust after treatment Dardiotis et al. [11] also performed a simulation study for the dynamic light-off scenario. Their simulations predicted that at comparable substrate dimensions and catalyst loading the filter is expected to show worse dynamic light-off behaviour than the flow-through monolith. In [12] this study was extended to zoned particulate filters.

More recently a number of modelling studies of the wall-flow filter have been published in the context of diesel particulate filters with wall integrated SCR catalyst functionality [13–16].

3. Methodology

3.1. Experimental

3.1.1. Catalyst samples

Conventional open monoliths and wall-flow filters were coated using an identical washcoat formulation. Cordierite substrates with square channels and a typical cell density and wall thickness (filter: 300 cpsi/12 mil, open monolith: 600 cpsi/4.3 mil) were used. In case of the open monolith the washcoat was deposited on top of the monolith wall as thin layer whereas the washcoat of the catalysed filter is assumed to be completely dispersed inside the porous wall. To be comparable, monolith and filter were prepared with identical washcoat loading (100 g L⁻¹) and precious metal loading (46 g ft⁻³ Pd; 4 g ft⁻³ Rh). Both catalyst samples were aged for 4 h at 925 °C in an atmosphere of 10 vol% H₂O in air.

3.1.2. Fast-light-off experiments

In the temperature step experiment the initially cold catalyst is subjected to the flow of the preheated inlet gas mixture by means of a switching valve. In this way the sample is heated up by the hot exhaust gas. The axial temperature profile in the catalyst is monitored by eight thermocouples placed inside the channels. The CO outlet concentration is measured with a mass spectrometer (V&F Analyse- und Messtechnik, AirSense2000).

Temperature profiles of a typical heat-up experiment with N₂ are shown in Fig. 1. Starting at room temperature, it can be seen that the exhaust gas reaches 95 % of the target temperature in about 5 s.

All light-off experiments reported in this paper were carried out with an exhaust mixture containing 5000 ppm (mol mol⁻¹) CO, 3000 ppm (mol mol⁻¹) O₂ and N₂ as gas balance. The inlet gas temperature was varied in a temperature range from 250 °C to 350 °C with a step size of 25 °C. The feed gas composition and temperature was held constant during each experiment. It was made sure

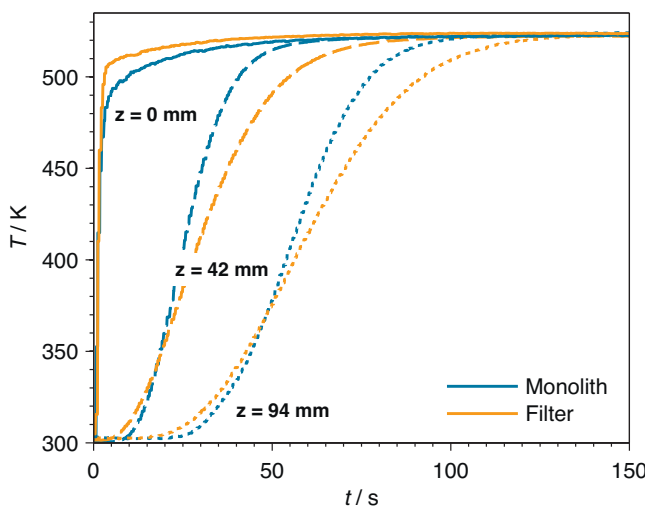


Fig. 1. Experimental temperature profiles for the conventional monolith and the catalysed filter at three axial positions (z), during heat-up with N_2 as exhaust gas.

that before each experiment the catalyst was cooled down to below 30 °C.

3.2. Simulation

3.2.1. Kinetic model

For the description of CO-oxidation a widely used global kinetic model introduced by Voltz et al. [17] is applied. This kinetic model is based on a LHHW approach and takes into account the inhibition effect of CO adsorption on the overall reaction rate.

Reaction rates are calculated using Eq. (1), where x_i is the mole fraction of gas species i , k_{CO} the rate constant for CO-oxidation and K_{ads} the adsorption constant for CO-adsorption on the catalyst surface.

$$r_{CO} = - \frac{k_{CO} \cdot x_{CO} \cdot x_{O_2}}{(1 + K_{ads} \cdot x_{CO})^2 \cdot T} \quad (1)$$

The temperature dependence of the rate constants is considered due to an Arrhenius approach. It is assumed that the three way catalyst washcoat is completely dispersed inside the porous wall of the filter. Because of the higher volume of the wall compared to the washcoat volume in the conventional monolith the active side density for the filter have to be adjusted.

3.2.2. 1D+1D model of the wall-flow filter

The reactor model used in this work solves the governing equations for the conservation of momentum, energy and mass for one representative pair of inlet and outlet channels and the corresponding wall. One-dimensional velocity, temperature and concentration profiles are computed for the inlet and outlet channel with radial transports effects described by the corresponding transfer coefficients. For each axial location the concentration profiles in the wall are resolved in radial direction whereas radial heat conduction is assumed to be fast so that one radially averaged temperature is computed for the wall. A schematic side and front view of the filter geometry implemented in the 1D+1D model is given in Fig. 2.

Momentum Transport: The one dimensional governing equation for momentum transport of the exhaust gas in the inlet ($j=1$) and the outlet ($j=2$) channel is described by:

$$\rho_j \cdot \frac{d}{dz} (v_j^2) = - \frac{dp_j}{dz} - F_j \cdot \frac{\eta_j \cdot v_j}{d_{channel}^2} \quad (2)$$

where v_j is the radially averaged gas velocity, p_j the average gas pressure and η_j the dynamic viscosity. F_j is the momentum transfer coefficient for fully developed laminar flow in a square tube ($F_j = 28.454$) [18].

Pressure Drop across the Porous Wall: The pressure drop across the porous wall, which couples the inlet and outlet channel, is calculated using the Darcy law Eq. (3) for porous media.

$$\Delta p = \frac{\eta \cdot u_{wall}}{k_{wall}} \cdot d_{wall} \quad (3)$$

Thereby k_{wall} is the wall permeability of the filter wall including the washcoat inside the pores. This combined wall permeability is determined by fitting the simulation model to pressure drop experiments. Therefore the filter's pressure drop was measured at different volume flows using the experimental setup described in [19]. Zero permeability is assumed for the plugs, which means that the wall velocity u_{wall} is forced to zero.

Gas Phase Heat Transfer: The energy transport equation in the gas phase is written as follows:

$$c_{p,j} \cdot \rho_j \cdot v_j \cdot \frac{dT_j}{dz} = \frac{4}{D_H} \cdot (T_{wall} - T_j) \cdot [\alpha_j + (-1)^j \cdot c_{p,j} \cdot \rho_j \cdot u_{wall}] \quad (4)$$

where D_H is the hydraulic diameter, T_{wall} the temperature of the porous wall and T_j the gas temperature in the inlet ($j=1$) and outlet ($j=2$) channel. The position dependent heat transfer coefficient α_j is computed from the Nusselt Number Nu using a correlation of Groppi et al. [20]. This correlation takes into account the effect of developing velocity and temperature profiles. In reality the gas-wall heat transfer in the particulate filter is a function of the radial flow velocity through the wall so that the use of a velocity independent heat transfer coefficient has to be regarded as an approximation. Recently Bissett and Kostoglou [21,22] provided a correlation equation that considers the effect of radial wall velocity and computes the heat and mass transfer coefficients as a function of the wall Reynolds number Re_w . It was found that the low flow rates used in this study result in very small wall Reynolds numbers Re_w so that the influence of suction and injection on the heat and mass transfer coefficient was neglected. This approximation will be further justified in Section 3.2.3 where the 1D+1D model will be compared to a model that solves the full 2D conservation equations for momentum, heat and mass. Therefore it does not rely on mass and heat transfer coefficients.

Solid Phase Energy Balance: The temperature field in the solid phase of the wall-flow filter is described by three different source terms. They include the contribution of convective heat transport of the gas flow through the wall, the heat transfer from the gas phase and the exothermic heat release:

$$c_{p,wall} \cdot \rho_{wall} \cdot \frac{dT_{wall}}{dt} = \dot{Q}_{convection} + \dot{Q}_{transfer} + \dot{Q}_{reaction} \quad (5)$$

$c_{p,wall}$ is the heat capacity of cordierite as a function of wall temperature. The wall density (ρ_{wall}) is computed using the deposited amount of washcoat, the substrate mass and the calculated volume of the porous wall. Taking into account the plugs additional thermal mass, there is an increased value of ρ_{wall} at the front and rear part of the wall. In case of the used catalyst sample (chapter 3.1.1) the plug's mass constitutes about 8 wt% of the total filter mass.

Convection of Heat: The convection of heat due to the flow from the inlet channel, through the wall into the outlet channel can be described by the following equation:

$$\dot{Q}_{convection} = \rho_{gas} \cdot c_{p,gas} \cdot u_{wall} \cdot \Phi \cdot T_{wall} \Big|_{x=0} - \rho_{gas} \cdot c_{p,gas} \cdot u_{wall} \cdot \Phi \cdot T_{wall} \Big|_{x=d_{wall}} \quad (6)$$

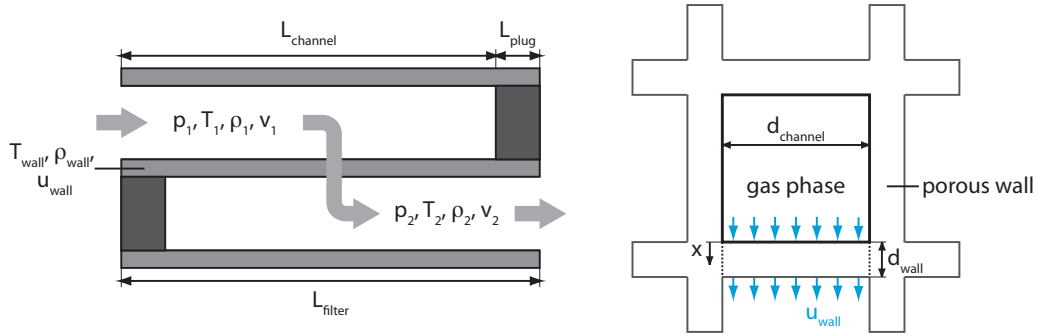


Fig. 2. Schematic of the 1D + 1D channel model with gas flow through the filter wall (left: side view; right: front view).

Under the assumption of wall temperature T_{wall} independent of the radial position x inside the wall, the convective terms will cancel out.

Heat Transfer from Channel Gas: In analogy to Eq. (4) the heat transfer from the channel gas to the filter wall is expressed using the above mentioned correlation to compute the position dependent heat transfer coefficient α_j .

$$\dot{Q}_{\text{transfer}} = \alpha_1 \cdot \Phi \cdot (T_1 - T_{\text{wall}}) + \alpha_2 \cdot \Phi \cdot (T_2 - T_{\text{wall}}) \quad (7)$$

Reaction Heat Source: The exothermic heat release is expressed by the following formula:

$$\dot{Q}_{\text{reaction}} = \Phi \cdot \int_0^{d_{\text{wall}}} r \cdot \Delta_r H \cdot dx \quad (8)$$

where r is the reaction rate and $\Delta_r H$ the reaction enthalpy of the associated reaction, integrated over the entire wall thickness d_{wall} and Φ is the specific filtration area per wall volume.

Gas Phase Mass Conservation: Concentration profiles along the inlet and outlet channel are computed using the following one dimensional mass conservation equation:

$$\frac{\partial c_j}{\partial t} = -v_j \cdot \frac{\partial c_j}{\partial z} - \beta_j \cdot \frac{4}{D_H} \cdot (c_j - c_{\text{wall}}) + (-1)^j \cdot u_{\text{wall}} \cdot \frac{4}{D_H} \cdot c_{\text{wall}} \quad (9)$$

v_j is the average gas velocity, c_j the concentration of the exhaust gas in the inlet ($j=1$) and the outlet ($j=2$) channel and c_{wall} the concentration at the wall surface. Because of the analogy between heat and mass transfer the mass transfer coefficient β_j is computed from the Sherwood Number Sh using the same correlation as for the Nusselt Number Nu [20].

To calculate the dynamic viscosity (η), heat capacity (c_p) and heat conductivity (k) for the gas phase, temperature-dependent polynomials were used. The required coefficients were fitted to experimental data sets for nitrogen (N_2) found in the literature [23]. Density (ρ) and inlet concentration ($c_{\text{in},0}$) are computed using the ideal gas law Eq. (10).

$$\rho = \frac{p \cdot M}{R \cdot T} \quad \text{and} \quad c_{\text{in},0} = x_0 \cdot \frac{p}{R \cdot T} \quad (10)$$

Radial Diffusion: To take into account radial diffusion effects of the gas species inside the porous wall, at each axial position the following radial mass transport equation is solved:

$$\frac{\partial c_{\text{wall}}}{\partial t} = \frac{\partial J_{\text{wall}}}{\partial x} + r \quad (11)$$

where c_{wall} is the concentration and r the reaction rate of the respective gas species. J_{wall} is the flux of the gas species along the radial coordinate x . According to Fick's law the fluxes in radial direction can be calculated as follows:

$$J_{\text{wall}} = -D_{\text{eff}} \cdot \frac{dc_{\text{wall}}}{dx} + u_{\text{wall}} \cdot c_{\text{wall}} \quad (12)$$

The boundary conditions for the mass transfer between the inlet channel and the porous wall is given in Eq. (13) and in direct analogy for the porous wall/outlet channel interface in Eq. (14).

$$D_{\text{eff}} \cdot \frac{dc_{\text{wall}}}{dx} \Big|_{x=0} = \beta_1 \cdot (c_{\text{wall}} \Big|_{x=0} - c_1) \quad (13)$$

$$D_{\text{eff}} \cdot \frac{dc_{\text{wall}}}{dx} \Big|_{x=d_{\text{wall}}} = \beta_2 \cdot (c_{\text{wall}} \Big|_{x=d_{\text{wall}}} - c_2) \quad (14)$$

Binary gas phase diffusion coefficients (D_{AB}) for CO in nitrogen are calculated via the semi empirical method of Fuller et al. [24]. The effective diffusion coefficients in the porous wall (D_{eff}) is computed using the parallel pore model Eq. (15), where ε is the materials porosity and τ the tortuosity, an empirical correction factor [25].

$$D_{\text{eff}} = \frac{\varepsilon}{\tau} \cdot D_{AB} \quad (15)$$

Experimental values for the effective wall diffusion coefficients for coated particulate filters were provided by Kroecher et al. [25]. The diffusion coefficients used in this study are in good agreement with the experimental values.

3.2.3. Validation of the 1D + 1D filter model

The 1D + 1D model described in section 3.2.2 relies on a number of simplifying assumptions such as:

- 1D treatment of the gas flow in the channels
- Description of radial heat and mass transfer in the channels by transfer coefficients that are assumed to be independent of the radial flow
- Neglect of axial heat conductance and diffusion

In order to validate these model assumptions and to verify the accuracy of the numerical solution procedure a 2D model of a particulate filter was implemented in the commercial simulation package COMSOL Multiphysics 3.3a. The 2D model assumes rotational symmetry for the inlet and outlet channel and solves the 2D equations for the flow field, temperature and concentration in the two channels and the porous wall.

A simple first order reaction was used for the model validation, since with the more complicated kinetic equation, applied in Section 3.2.1, in some cases no stable numerical solution could be obtained by COMSOL. For the comparison of the two models, in the 1D + 1D model the transfer coefficients for momentum, heat and mass in Eqs. (2, 4, 7 and 9) were replaced by the corresponding coefficients for circular channels.

Fig. 3 compares simulation results of the 1D + 1D model and the 2D model for a typical validation case. Very good agreement between the two models is obtained for the outlet concentrations (Fig. 3a) and the computed wall temperatures (Fig. 3b). On the whole, for all test cases considered during the validation study, the

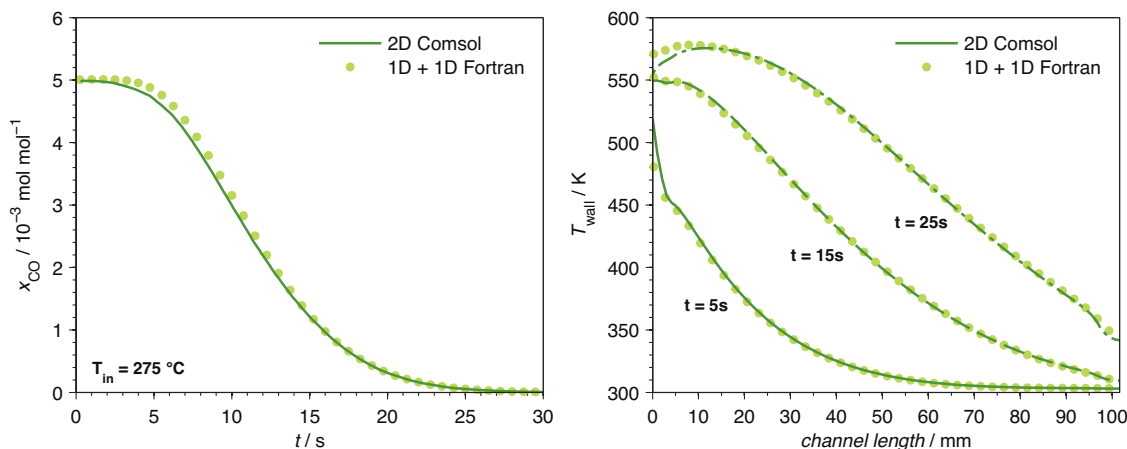


Fig. 3. Validation of the 1D + 1D model against the full 2D solution of the conservation equations. Left: CO-emissions at reactor outlet. Right: Axial temperature profiles. Operating conditions: 5000 ppm CO, 3000 ppm O₂, GHSV: 20000 h⁻¹, T_{in} : 275 °C.

agreement of the two models was found to be acceptable, especially if compared to the expected uncertainty of the laboratory experiment.

3.2.4. 1D + 1D model of the flow-through monolith

The model of the flow through monolith solves the heat and mass balance equations for one representative channel of the monolith. The flow in the open channel is considered as one dimensional so that the gas phase temperature T_{gas} and concentration $c_{gas,i}$ of the gas species i are computed as velocity averaged quantities. Radial transport in the gas phase is described by heat and mass transfer coefficients. Concentration profiles in the gas phase are computed according to:

$$\frac{\partial c_{gas,i}}{\partial t} = -v_{gas} \cdot \frac{\partial c_{gas,i}}{\partial z} - \beta_i \cdot \frac{4}{D_H} \cdot (c_{gas,i} - c_{wc,i}) \quad (16)$$

where v_{gas} is the average gas velocity, D_H the hydraulic diameter and $c_{wc,i}$ the concentration of species i at the washcoat surface. The position dependent mass transfer coefficient β_i is computed from the Sherwood Number:

$$Sh = \frac{\beta_i \cdot D_H}{D_i} \quad (17)$$

where D_i is the diffusion coefficient of species i in nitrogen, calculated using a the semi empirical method of Fuller et al. [24]. Taking into account the effect of developing concentration profiles the position dependent Sherwood Number Sh is computed, following a correlation from [26].

In order to consider diffusion limitations in the washcoat, radial concentration profiles for each axial position in the washcoat are computed by solving the following mass transport equation:

$$\frac{\partial c_{wc,i}}{\partial t} = \frac{\partial J_{wc,i}}{\partial x} + r_i \quad \text{with} \quad J_{wc,i} = -D_{eff,i} \cdot \frac{\partial c_{wc,i}}{\partial x} \quad (18)$$

Where $c_{wc,i}$ is the concentration, r_i the reaction rate and $D_{eff,i}$ the effective diffusion coefficient in the washcoat of the respective gas species i . $J_{wc,i}$ is the flux of the gas species along the radial coordinate x . The boundary condition for the mass transfer between the gas phase and the washcoat is given in Eq. (19).

$$D_{eff,i} \cdot \frac{dc_{wc,i}}{dx} \Big|_{x=0} = \beta_i \cdot (c_{wc,i}|_{x=0} - c_{gas,i}) \quad (19)$$

The gas phase temperature T_{gas} and the substrate temperature T_s are computed by solving the heat balance equations:

$$\frac{\partial T_{gas}}{\partial t} = -v_{gas} \cdot \frac{\partial T_{gas}}{\partial z} - \alpha \cdot \frac{4}{D_H \cdot \rho_{gas} \cdot c_{p,gas}} \cdot (T_{gas} - T_s) \quad (20)$$

$$\frac{dT_s}{dt} = \Phi \cdot \frac{\alpha}{\rho_s \cdot c_{p,s}} \cdot (T_{gas} - T_s) + \Phi \cdot \frac{1}{\rho_s \cdot c_{p,s}} \cdot \int_0^{d_{wc}} r \cdot \Delta_r H \cdot dx \quad (21)$$

where r is the reaction rate, $\Delta_r H$ the reaction enthalpy of the associated reaction, integrated over the entire washcoat thickness d_{wc} and Φ is the specific surface area between gas and solid per wall volume.

A more detailed description of the monolith reactor model can be found in [27,28].

4. Results and discussion

4.1. Filter versus open monolith: Experimental comparison of the dynamic cold start performance

Temperature step experiments were used to experimentally compare the dynamic light-off performance of a wall-flow filter and a conventional open monolith. Experiments were performed for a filter and an open monolith with identical washcoat, precious metal loading and overall thermal capacity. Results at four different inlet temperatures are shown in Fig. 4. In all cases the conventional open monolith shows a faster light-off compared to the catalysed filter. This delayed light-off for the filter results in significantly increased cumulated CO emissions. Table 1 summarises the observed increase in the cumulated CO emissions for the filter configuration relative to the conventional open monolith. At 250 °C the cumulated CO emissions of the catalysed filter exceed the emissions of the open monolith by 190%. At 325 °C the filter shows nearly three times the emissions of the open monolith.

Table 1

Comparison of the cumulated emissions obtained for the conventional monolith and the catalysed filter during temperature step experiments at four different gas inlet-temperatures (open monolith = 100%).

Gas inlet temperature/°C	Relative cumulated CO emissions/%
Catalysed filter	
250	190
275	210
300	300
325	299

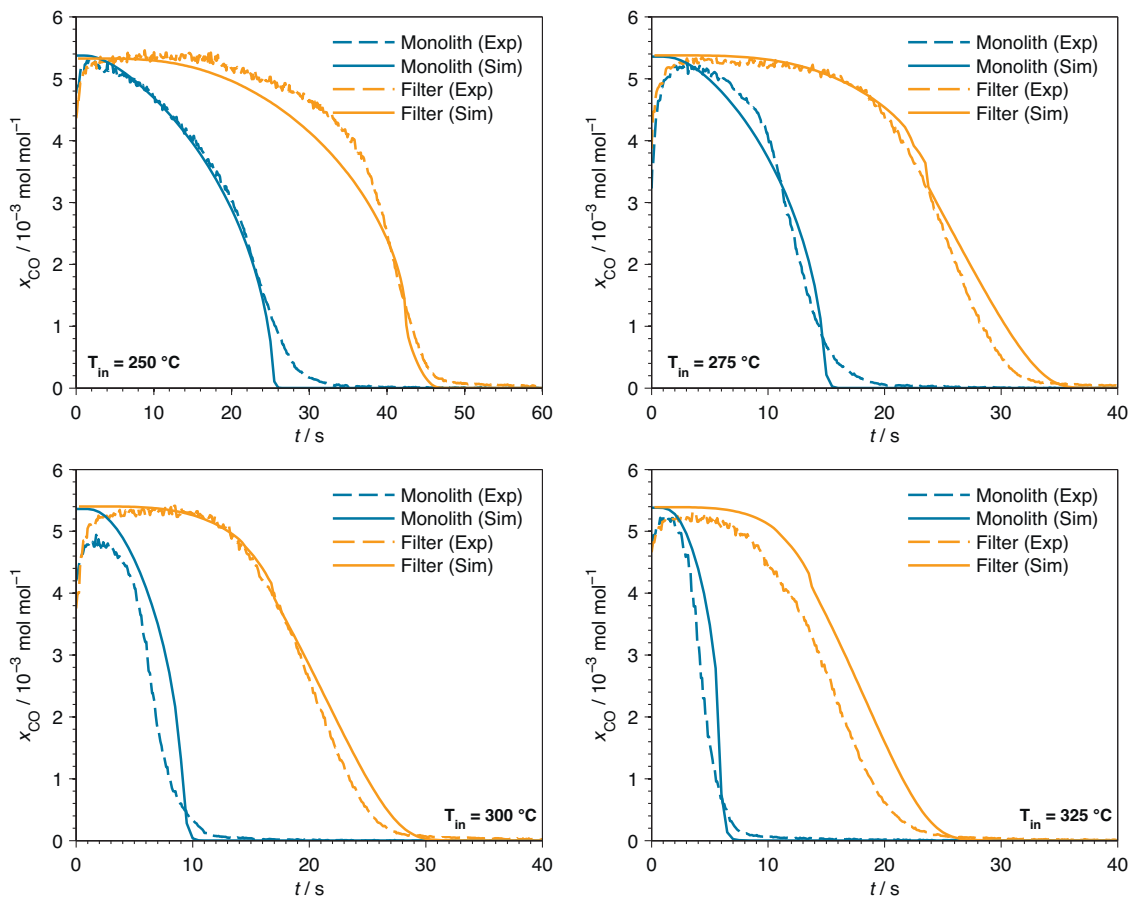


Fig. 4. Comparison of the fast-light-off performance for the conventional monolith and the catalysed filter. Experiment versus model prediction. Mole fraction of CO at the outlet of the catalyst plotted against time at four gas inlet-temperatures in the range from 250 °C to 325 °C (5000 ppm CO, 3000 ppm O₂, GHSV: 20000 h⁻¹).

4.2. Experiments versus model prediction

In this section it is investigated in how far the experimentally observed difference in the cold-start performance between catalysed filter and open monolith can be predicted by the simulation model. To this end a kinetic model for the CO oxidation is parameterised in Section 4.2.1 using only experimental data obtained for the flow-through monolith. Without further parameter adjustment this kinetic model is applied in the filter model to predict the dynamic light-off performance of the catalysed gasoline particulate filter (Section 4.2.2).

4.2.1. Parameterisation of the CO oxidation kinetics for the open monolith

The parameterisation of the kinetic model for the applied three way catalyst washcoat is carried out using experimental data obtained by 'fast light-off' experiments with the conventional flow-through monolith. Measurements at five gas inlet-temperatures were used for the model parameterisation. Besides the pre-exponential factor $A_{0,\text{Oxidation}}$ and the activation energy $E_{A,\text{Oxidation}}$ for the CO oxidation, also the pre-exponential factor $A_{0,\text{Adsorption}}$ and the activation energy $E_{A,\text{Adsorption}}$ in the inhibition term were adjusted. The parameter optimisation was carried out using a non-linear least squares method, fitting the flow-through monolith model described in Section 3.2.4 to the experimentally obtained CO emissions at the outlet of the catalyst. The results of the optimisation for five gas inlet-temperatures are shown in Fig. 5.

A good agreement between experiment and simulation is obtained over the entire temperature range. The kinetic parameters obtained from the parameter fit are provided in Table 2.

4.2.2. Model prediction of the filter's cold-start performance

The kinetic model that was parameterised in Section 4.2.1 was implemented in the filter model without any further adjustment of the kinetic parameters. The simulation results and the corresponding experimental data at four gas inlet-temperatures are shown in Fig. 4. CO emissions at the outlet of the catalysed filter are nearly quantitatively predicted by the numerical simulation. This means that the experimentally observed difference in the cumulated CO emissions between open monolith and catalysed filter is well described by the model.

Fig. 6 compares the computed axial temperature profiles in the filter and the open monolith to experimental data. Obviously the measured temperature profiles for both reactor configurations are well reproduced by the model. Compared to the catalysed filter, a more pronounced exothermic temperature increase is observed in

Table 2

Kinetic parameters for the applied three way catalyst washcoat obtained by experimental data of the conventional flow-through monolith.

Kinetic parameter		
$A_{0,\text{Oxidation}}$	1.2731×10^{17}	s^{-1}
$E_{A,\text{Oxidation}}$	52.72	kJ mol^{-1}
$A_{0,\text{Adsorption}}$	3.7843×10^2	s^{-1}
$E_{A,\text{Adsorption}}$	-12.67	kJ mol^{-1}

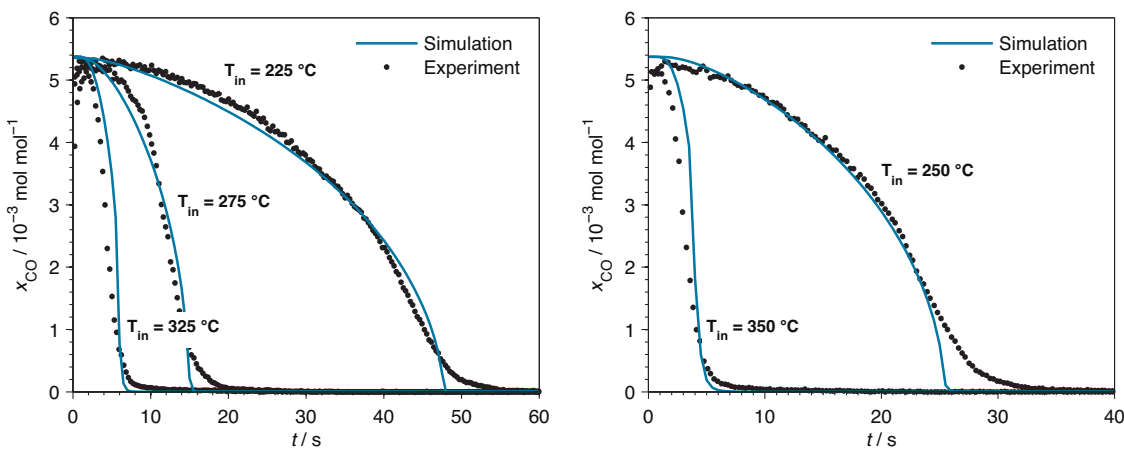


Fig. 5. Parameterisation of the kinetic model using 'fast light-off' experiments with the open monolith. CO mole fractions at reactor outlet plotted against the time. Operating conditions: 5000 ppm CO, 3000 ppm O₂, GHSV: 20 000 h⁻¹.

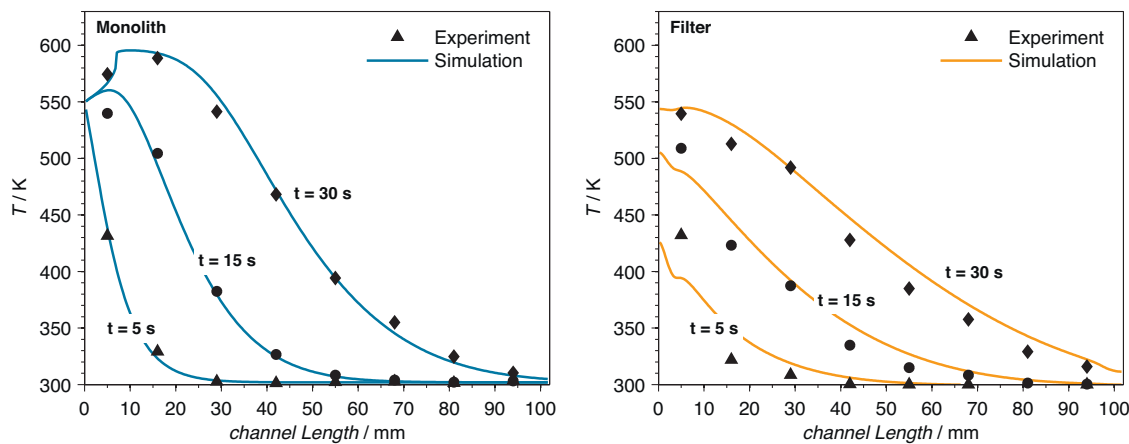


Fig. 6. Comparison of the axial temperature profiles along the channel length obtained for the open monolith (left) and the wall-flow filter (right) at three points in time (T_{in} : 275 °C, 5000 ppm CO, 3000 ppm O₂, GHSV: 20 000 h⁻¹).

the inlet part of the open monolith. Also this effect is well reproduced by the model.

4.3. Sensitivity analysis

In the previous section we have shown that the experimentally observed differences between the filter and the open monolith are well predicted by the numerical simulation. This provides confidence that the model indeed correctly captures the underlying physics of the light-off process. In the following the simulation model is applied in a sensitivity analysis in order to identify and quantify the individual physical phenomena that are responsible for the observed differences in light-off performance between the open monolith and the catalysed filter.

4.3.1. The effect of thermal mass

To study the effect of the filters thermal mass on the cold-start performance, simulations were carried out where the heat capacity of the filter material was systematically varied between 80% and 115% of its nominal value, see Fig. 7. As expected, heat capacity has a significant influence on the light-off performance of the catalysed filter. A reduction of the thermal mass by 20% will decrease the cumulated CO emissions for the temperature step experiment at 275 °C by 17.5%. This means that the reduction of the filter's thermal mass is one promising direction for the future development of gasoline particulate filters with improved

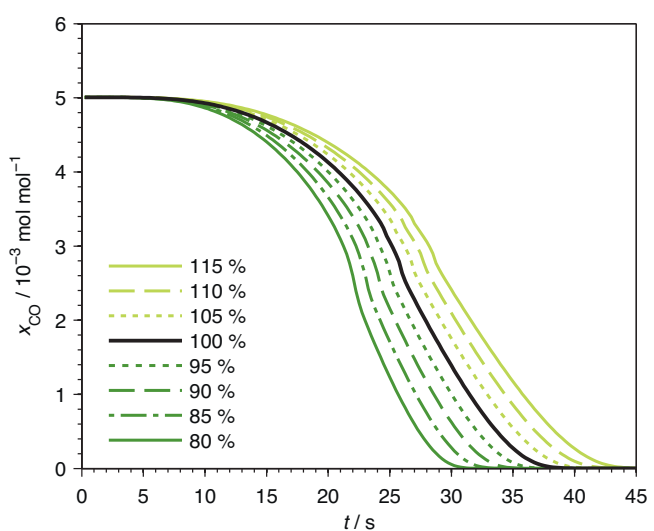


Fig. 7. Influence of thermal mass of the Light-Off behaviour: CO mole fractions at the outlet of the catalysed filter plotted against the time. Fast-light-off performance for the catalysed filter with a systematically varied thermal mass in the range of 80% to 115% of the nominal value (5000 ppm CO, 3000 ppm O₂, GHSV: 20 000 h⁻¹, T_{in} : 275 °C).

Table 3

Cumulated CO emissions for the filter and the open monolith with two different cell densities during the cold-start.

	Cumulated CO emissions/mmol	
	275 °C	400 °C
Monolith (600 cpsi)	6.05	1.38
Monolith (300 cpsi)	7.32	2.14
Filter	12.46	6.05

cold-start performance. Possible measures that could reduce the heat capacity would include a reduction of wall thickness or an increase in wall porosity, potentially in combination with the application of membrane concepts [29–31].

In the current study the open monolith and the catalysed filter were compared at an identical nominal thermal mass so that the experimentally observed differences in the light-off performance cannot be explained by thermal mass effects. Due to production tolerances the actual weight of the filter was 4.3 % higher than the weight of the open monolith (monolith: 180.9 g, filter: 188.7 g). According to the results of the sensitivity study presented in Fig. 7, a difference of 4.3 % in thermal mass should result in an increase of the cumulated CO emissions of less than 5 %, an order of magnitude lower than the experimentally observed increase by 110 %. In the following sections of this sensitivity study, the filter and the open monolith are compared at an identical thermal mass.

4.3.2. Effect of cell density

In the experimental study in Section 4.1 a catalysed filter with a cell density of 300 cpsi is compared to an open monolith with a higher cell density of 600 cpsi. The reason for using different cell densities for the filter and the open monolith is that in practice, due to backpressure considerations, particulate filters cannot be used with the high cell densities of today's open monoliths.

A dynamic cold-start was simulated for an open monolith with a cell density of 300 cpsi instead of the original 600 cpsi. For this simulation the entire cell, wall and washcoat geometry was scaled up. In this way not only the cell density of the open monolith was adjusted to that of the filter but also a comparable total wall thickness (304.8 μm for the open monolith including washcoat versus 304.8 μm for the filter wall) and open channel diameter is obtained. Simulation results for the open monolith with the adjusted cell density are shown in Fig. 8 at two different temperatures. Obviously, the reduced cell density leads to a significant deterioration of the monolith's light-off behaviour. The cumulated CO emissions resulting from the concentration profiles in Fig. 8 are summarised in Table 3. Based on the cumulated emissions of Table 3 the relative contribution of the cell density effect to the total experimentally observed difference in cold-start performance can be quantified as follows:

$$\text{rel. contribution of cell density} = \frac{n_{\text{mono},300\text{cpsi}} - n_{\text{mono},600\text{cpsi}}}{n_{\text{filter}} - n_{\text{mono},600\text{cpsi}}} \quad (22)$$

At 275 °C, 19.8 % of the difference in the experimentally observed cumulated CO emissions can be attributed to the cell density effect. At 400 °C the cell density effect accounts for 16.3 % of the total difference between filter and open monolith.

4.3.3. Thermal capacity of the plugs

The plugs only contribute ~8 % of the thermal mass of the catalysed filter. Nevertheless, the presence of the plugs increases the thermal mass of the first 4 mm of the filter's channel by ~100 %. Due to inlet effects, the first millimetres of the channel in the open monolith heat up particularly fast and have a large contribution to the initial light-off. To quantify the negative effect of the plugs on

Table 4

The relative contribution of the different effects to the total difference in the cumulated CO emissions between the filter and the open monolith. The relative contribution of the individual effect was calculated in analogy to Eq. (22).

Geometric effect	Rel. contr. to total difference in cum. CO emissions/%	
	275 °C	400 °C
Cell density	19.8	16.3
Thermal capacity of plugs	40.0	34.3
Intrinsic difference	40.2	49.4

the filters light-off behaviour, simulations were carried out for a filter with infinitesimally short plugs. In these simulations the heat capacity of the filter wall was appropriately increased so that the total thermal mass of the filter was kept constant. Fig. 9 compares axial temperature profiles for a filter with 4 mm long plugs and for a filter with infinitesimally short plugs. Obviously, the thermal mass of the plugs significantly lowers the wall temperature in the inlet zone of the filter.

The effect of the plug's thermal mass on the CO emissions during cold-start is shown in Fig. 8. The cumulated CO emissions are summarised in Table 4. It can be seen that the thermal capacity of the plugs has a significant influence on the filters CO emissions during cold-start. The relative contribution of the plug effect to the experimentally observed difference in the cumulated CO emissions can be computed in analogy to Eq. (22). At 275 °C, 40.0 % of the experimentally observed difference between filter and open monolith can be attributed to the plug effect. At 400 °C the plug effect still accounts for 34.3 % of the total difference.

4.3.4. Intrinsic differences between the open monolith and the catalysed filter

Table 4 and Fig. 8 show that a significant part of the experimentally observed differences in the cold-start behaviour between the catalysed filter and the open monolith can be attributed to the effects of cell density and the thermal capacity of the plugs. However the results also demonstrate that the open monolith still shows a significantly better light-off performance compared to the catalysed filter, if catalysed filter and open monolith are compared at identical cell density and without the effect of the plugs. This intrinsic difference must be attributed to the different specific interactions of heat transfer, mass transport and reaction in the two reactor configurations. In this section we aim at further elucidating the physical origin of these intrinsic differences. For this purpose in the following sections a filter with infinitesimally short plugs (III) and an open monolith (I), both with identical cell density of 300 cpsi, are used as reference cases. Simulations are then carried out where the effects of heat transfer, external and internal mass transfer are individually eliminated in the simulation so that the contribution of the individual effects to the observed difference in the cold-start performance can be quantified.

4.3.4.1. The effect of heat transfer. Fig. 10 compares axial temperature profiles in the open monolith (I) and in the wall-flow filter with infinitesimal short plugs (III) during the transient heat-up with pure nitrogen. The simulations show that compared to the open monolith, in the catalysed filter the temperature increase is distributed over a broader zone in axial direction with lower peak temperatures at the channel inlet. This result can be explained by the fact that in the catalysed filter only half the channels are inlet channels contributing to the heat transfer from the gas phase to the filter walls. Therefore (at equal temperature difference between gas and wall) the overall heat transfer per reactor volume in case of the filter is only half that of the open monolith. In order to take this effect into account, simulations were carried out for the catalysed filter

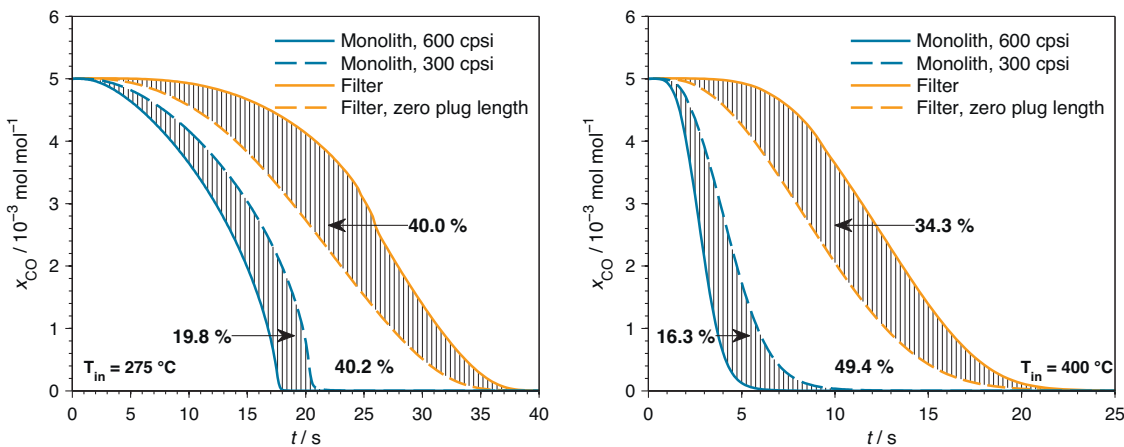


Fig. 8. Sensitivity analysis: The effect of cell density and the plugs' thermal mass. CO mole fractions at reactor outlet plotted against time for a gas inlet temperature of $275\text{ }^{\circ}\text{C}$ (left) and $400\text{ }^{\circ}\text{C}$ (right). Contribution of the geometric effects to the observed difference in the light-off performance (5000 ppm CO, 3000 ppm O₂, GHSV: 20000 h^{-1}).

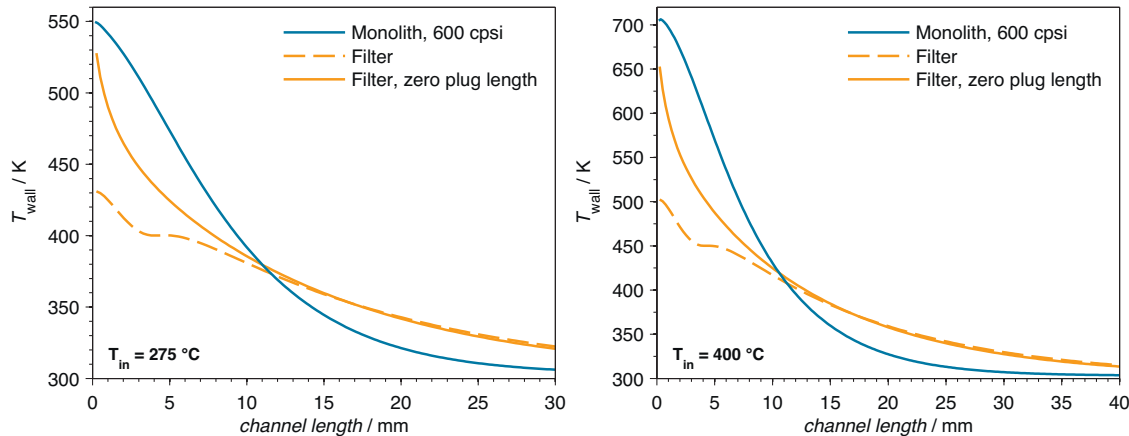


Fig. 9. The effect of the plugs' thermal mass on the axial temperature profile. Simulated wall temperature for the open monolith, the catalysed filter and the filter with infinitesimal plug length, 5 s after the fast-light-off experiment was started, plotted against the axial position. The simulation conditions are 5000 ppm CO, 3000 ppm O₂, GHSV: 20000 h^{-1} and gas inlet-temperatures of $275\text{ }^{\circ}\text{C}$ (left) and $400\text{ }^{\circ}\text{C}$ (right).

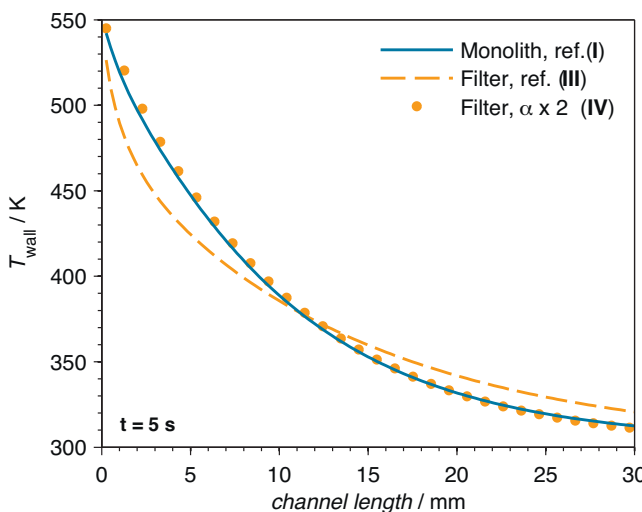


Fig. 10. The effect of gas-wall heat transfer on the axial temperature profiles. Temperature profiles for the heat-up in pure nitrogen depicted 5 s after the temperature step experiment was started. (I) open monolith, 300 cpsi; (III) filter, infinitesimal short plugs; (IV) same as III but heat transfer coefficient $\times 2$ (100% N₂, GHSV: 20000 h^{-1} , T_{in} : $275\text{ }^{\circ}\text{C}$).

with the heat transfer coefficient multiplied by a factor of two (IV). With the doubled heat transfer coefficient, the temperature profile of the filter indeed closely resembles the temperature profile obtained for the open monolith. On the one hand this confirms that the heat transfer per reactor volume is reduced by half in case of the wall-flow filter. On the other hand this result implies that for the purpose of a sensitivity study, the effect of heat transfer can be eliminated by doubling heat transfer coefficient of the filter by a factor of two.

Fig. 11 compares the CO emissions for reference simulations of the open monolith (I) and the filter (III) with a simulation of the filter where the heat transfer coefficient was multiplied by a factor of two (IV). The cumulated emissions for the different simulations are summarised in Table 5. Obviously, eliminating the differences in heat transfer through an increased heat transfer coefficient significantly reduces the cumulated CO emissions of the filter. The relative contribution of the heat transfer effect to the total intrinsic difference between the filter and the open monolith can be computed in analogy to Eq. (22). At $275\text{ }^{\circ}\text{C}$, 67.7% of the intrinsic difference in the cumulated emissions between the open monolith and the filter can be attributed to heat transfer effects. At $400\text{ }^{\circ}\text{C}$, the heat transfer effect still contributes 36.4% of the total difference between filter and conventional monolith.

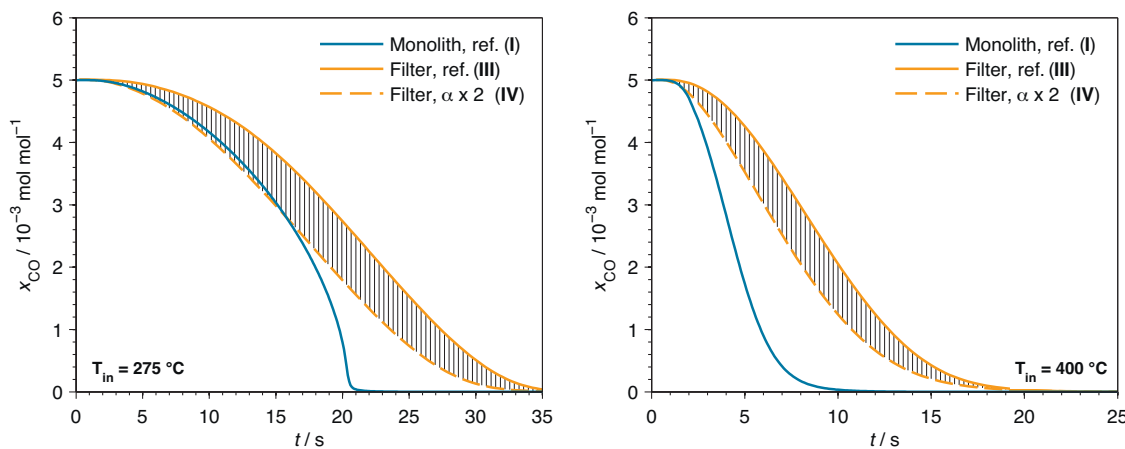


Fig. 11. Sensitivity analysis: The effect of gas-wall heat transfer on the light-off behaviour. CO mole fractions at reactor outlet plotted against the time at 275 °C and 400 °C. (I) open monolith, 300 cpsi; (III) filter, infinitesimal short plugs; (IV) same as III but heat transfer coefficient $\times 2$ (5000 ppm CO, 3000 ppm O₂, GHSV: 20000 h⁻¹).

4.3.4.2. The effect of diffusion resistance in the filter wall. To analyse the influence of diffusion resistance in the washcoat and in the filter wall, simulations were carried out, where the effective radial diffusion coefficient (D_{eff}) in the washcoat (II) and in the filter wall (V) was increased by a factor of 100. It was verified that with the increased diffusion coefficient radial gradients in the washcoat and in the filter wall completely vanished. Simulation results with and without the increased effective diffusion coefficient (D_{eff}) are compared in Fig. 12. Cumulated emissions for the different simulation runs are summarised in Table 5. Obviously, the light-off of the conventional flow-through monolith shows little effect of internal diffusion resistance. On the other hand, a significantly faster light-off is observed for the wall-flow filter if the internal diffusion limitation in the filter wall (V) is removed. As expected, the effect of internal diffusion limitation increases with temperature since the reactor is kinetically controlled at low temperature and there is a gradual transition to a more diffusion controlled operation at higher temperature. At 400 °C internal diffusion limitation accounts for more than half of the observed performance difference between the catalysed filter (III) and the open monolith (I), compare Table 6.

The main reason for the increased importance of internal diffusion limitations in case of the wall-flow filter can be seen in the higher diffusion length in the filter wall compared to the relatively thin washcoat layer.

The effect of internal diffusion limitation on the cold-start of the catalysed filter is further illustrated in Fig. 13 that shows 2D temperature and CO concentration profiles 7.5 s after the temperature step. At this point of time, the first few millimetres of the catalysed filter are sufficiently heated up so that the exhaust gas that flows through this part of the wall shows about 100% CO conversion. The

filter wall in the rear part of the filter is still cold, so that the CO that passes the wall in this cold zone cannot be converted. In the hot front part of the wall a steep gradient of the CO concentration is observed near the gas-wall interface, a clear indication of internal diffusion resistance effects.

4.3.4.3. The effect of external diffusion in the open channel. In the filter only every second channel is available as an inlet channel. In analogy to the discussion of heat transfer effects in Section 4.3.4.1 it can be assumed that (at identical concentration differences) the mass transfer per reactor volume in case of the filter will be half that of the open monolith. The effect of the reduced mass transfer rate in the filter reactor can be quantified by conducting a simulation of the filter with the mass transfer coefficient multiplied by a factor of two (VI). Results of such simulations are shown in Fig. 14, the corresponding cumulated CO emissions are reported in Table 5.

Obviously, differences in external mass transfer only provide a minor contribution to the observed overall performance difference between the filter and the open monolith. At 400 °C, the effect accounts for only 15.2% of the total intrinsic difference between the two reactor configurations. At 275 °C, the effect is even smaller, compare Table 6.

4.3.4.4. The combined effect of heat and mass transfer. As a final cross check the combined effects of heat transfer, internal and external mass transfer on the filter's light-off were investigated. To this end a simulation of the filter was conducted, where at the same time the heat- and mass transfer coefficients were multiplied by two and the effective diffusion coefficient in the filter wall was multiplied by 100 (VII). In this way the effects of heat transfer, external mass transfer and internal mass transfer limitation

Table 5

Cumulated CO emissions in mmol for the respective simulation during the light-off. Investigation of the isolated effects at 275 °C and 400 °C.

	Cumulated CO emissions / mmol	
	275 °C	400 °C
I Open monolith, 300 cpsi	7.32	2.14
II Same as I but $D_{eff} \times 100$	7.39	1.96
III Filter, 300 cpsi, infinitesimal short plugs	9.89	4.45
IV Same as III but heat transfer coefficient $\times 2$	8.15	3.61
V Same as III but $D_{eff} \times 100$	9.44	3.16
VI Same as III but mass transfer coefficient $\times 2$	9.66	4.10
VII Same as III but mass/heat transfer coefficient $\times 2$ and $D_{eff} \times 100$	7.49	1.85

Table 6

The relative contribution of the different effects to the total difference in the cumulated CO emissions between the filter and the open monolith. The relative contribution of the individual effects was calculated in analogy to Eq. (22).

Physical effects	Rel. contr. to total diff. in cum. CO emissions / %	
	275 °C	400 °C
Heat transfer (filter)	67.7	36.4
Internal mass transfer (filter)	17.5	55.8
Internal mass transfer (monolith)	2.7	-7.8
External mass transfer (filter)	9.0	15.2
Total	96.9	99.6

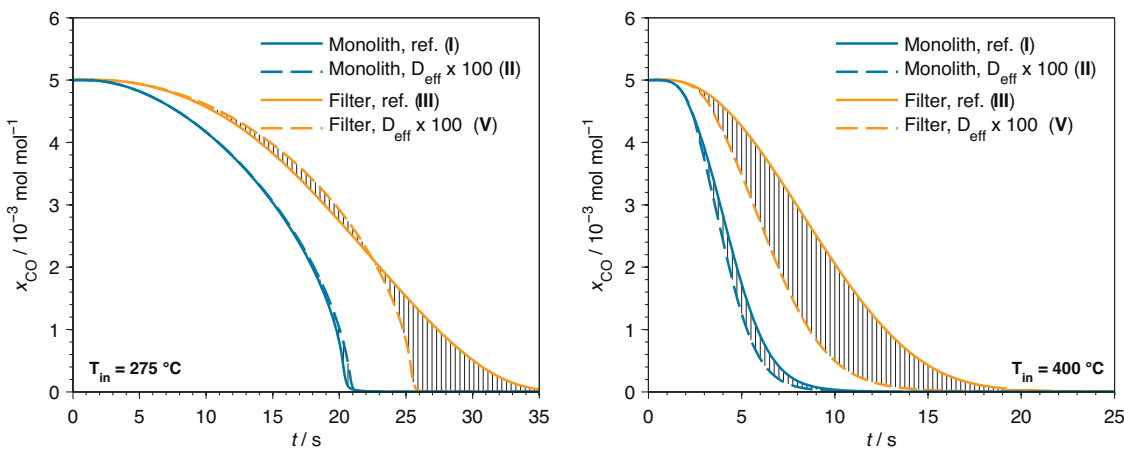


Fig. 12. Sensitivity analysis: The effect of diffusion limitations in the washcoat/wall on the light-off behaviour. CO mole fractions at the reactor outlet plotted against time at 275 °C and 400 °C. (I) open monolith, 300 cpsi; (II) same as I but $D_{\text{eff}} \times 100$; (III) filter, infinitesimal short plugs; (V) same as III but $D_{\text{eff}} \times 100$. (5000 ppm CO, 3000 ppm O₂, GHSV: 20000 h⁻¹).

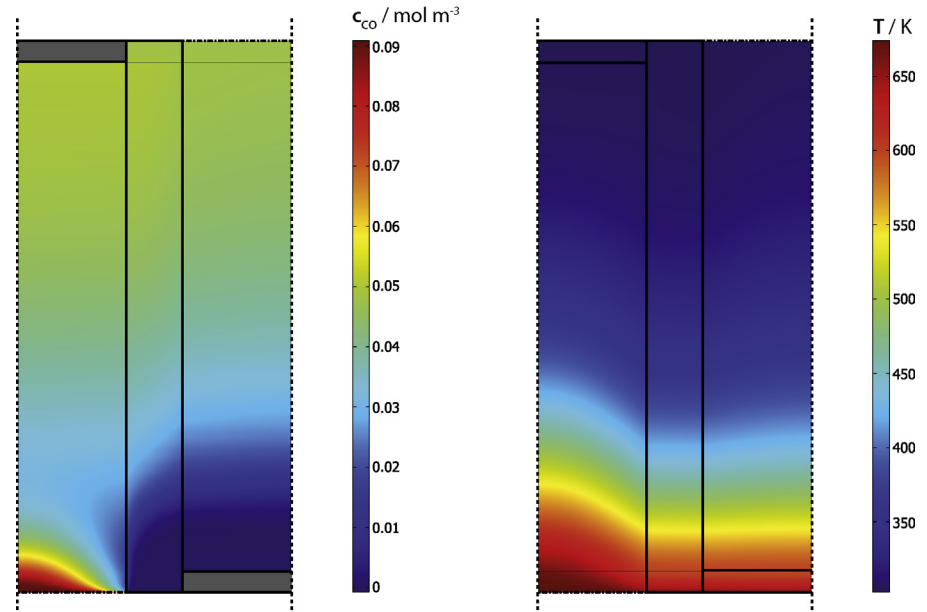


Fig. 13. Two-dimensional CO concentration (left) and temperature (right) profiles 7.5 s after the temperature jump from 20 to 400 °C. The simulation was carried out with the 2D model described in Section 3.2.3.

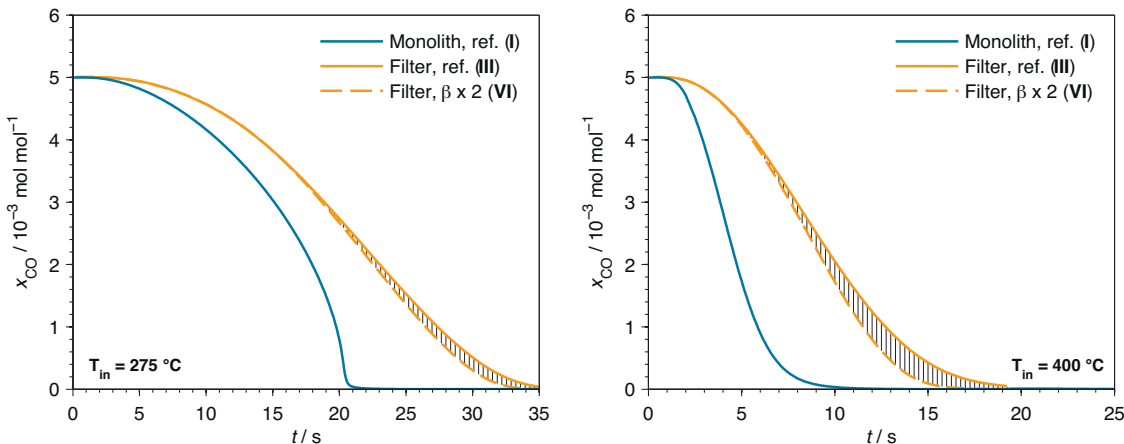


Fig. 14. Sensitivity analysis: The effect of gas-wall mass transfer on the light-off behaviour. CO mole fractions at the reactor outlet plotted against time at 275 °C and 400 °C. (I) open monolith, 300 cpsi; (III) filter, infinitesimal short plugs; (VI) same as III but mass transfer coefficient $\times 2$. (5000 ppm CO, 3000 ppm O₂, GHSV: 20000 h⁻¹).

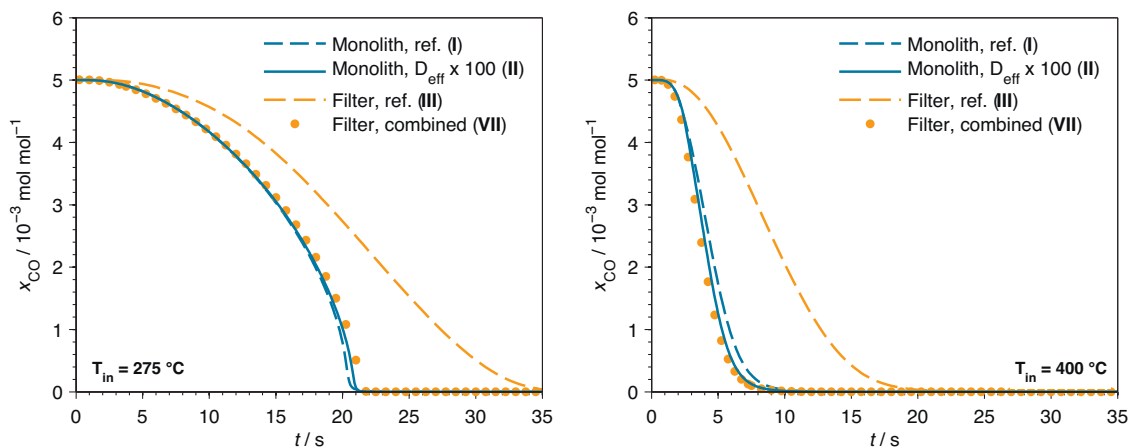


Fig. 15. Sensitivity analysis: The combined effect of heat and mass transfer. CO mole fractions at reactor outlet plotted against time at 275 °C and 400 °C. (I) open monolith, 300 cpsi; (II) same as I but $D_{eff} \times 100$; (III) filter, infinitesimal short plugs; (VII) same as III but mass/heat transfer coefficient $\times 2$ and $D_{eff} \times 100$. (5000 ppm CO, 3000 ppm O₂, GHSV: 20 000 h⁻¹).

where simultaneously compensated for as discussed in Sections 4.3.4.1–4.3.4.3. The result of this simulation is shown in Fig. 15, the cumulated CO emissions are reported in Table 5.

Obviously, if all three physical effects are compensated for (VII), the CO emissions of the filter reactor very well coincide with the CO emissions of the open monolith (I). An even slightly better agreement is obtained, if also in the open monolith internal diffusion limitation is eliminated by an increased effective diffusion coefficient (II).

This result suggests that the combined effects of heat transfer, external and internal mass transfer limitations indeed quantitatively explain the intrinsic difference in the light-off behaviour between the particulate filter (III) and the conventional open monolith (I).

5. Conclusion

Temperature step experiments were used to compare the cold-start performance of a conventional three way catalyst and a catalysed gasoline filter, both with an identical thermal mass and coated with the same washcoat. A significantly delayed light-off was observed for the particulate filter compared to the conventional open monolith. The resulting cumulated CO emissions of the catalysed filter exceed those of the open monolith by 190–300% in the temperature range between 250 °C and 325 °C.

A numerical simulation model for the gasoline particulate filter was presented and it was demonstrated that the experimentally observed difference in the light-off performance between the filter and the open monolith is well described by the model. In a first step the kinetics of CO oxidation were parameterised using only experimental data for the conventional flow-through monolith. When these kinetics were implemented in the filter model, the model quantitatively predicted the cold-start behaviour of the catalysed filter, without further adaptation of the kinetic parameters.

One motivation for the development of detailed reactor models is that these models provide an insight into the physical effects controlling the reactor performance. In our case, a sensitivity analysis revealed that a significant part of the experimentally observed performance difference between the filter and the open monolith can be explained by the higher channel diameter of the filter. Furthermore, the thermal capacity of the plugs and the corresponding delay in the heat up of the filter's inlet zone could be identified as

another important effect contributing to the delayed cold-start of the filter. Even if a filter and an open monolith are compared with an identical channel diameter and without the plug effect, simulation predicts a significantly faster light-off for the open monolith. This intrinsic difference in the cold-start performance could be quantitatively explained by the specific contributions of heat transfer, internal mass transfer and external mass transfer in the two reactor configurations.

References

- [1] C.L. Myung, S. Park, Int. J. Automot. Technol. 13 (2012) 9–22.
- [2] D. Dockery, C. Pope, X. Xu, J. Spengler, J. Ware, M. Fay, B. Ferris, F. Speizer, New Engl. J. Med. 329 (1993) 1753–1759.
- [3] U. Lahl, W. Steven, Gefahrst. Reinhal. L. 64 (2004) 325–331.
- [4] W. Piock, G. Hoffmann, A. Berndrofer, P. Salemi, B. Fusshoeller, SAE Tech. Pap. (2011), 2011-01-1212.
- [5] M. Braisher, R. Stone, SAE Tech. Pap. 201 (2010), 2010-01-0786.
- [6] C. Saito, T. Nakatani, Y. Miyairi, K. Yuuki, M. Makino, H. Kurachi, W. Heuss, T. Kuki, Y. Furuta, P. Kattouah, C.-D. Vogt, SAE Tech. Pap. SP-2318 (2011) 263–273, Special Publication.
- [7] J.-M. Richter, R. Klingmann, S. Spiess, K.-F. Wong, SAE Tech. Pap. (2012), 2012-01-1244.
- [8] S. Spiess, K.-F. Wong, J.-M. Richter, R. Klingmann, Top. Catal. 56 (2013) 434–439.
- [9] J.F. Knoth, A. Drochner, H. Vogel, J. Gieshoff, M. Koegel, M. Pfeifer, M. Votsmeier, Catal. Today 105 (2005) 598–604.
- [10] M. Votsmeier, J. Gieshoff, M. Koegel, M. Pfeifer, J.F. Knoth, A. Drochner, H. Vogel, Appl. Catal. B 70 (2007) 233–240.
- [11] C.K. Dardiotis, O.A. Haralampous, G.C. Koltsakis, Ind. Eng. Chem. Res. 45 (2006) 3520–3530.
- [12] C.K. Dardiotis, O.A. Haralampous, G.C. Koltsakis, Chem. Eng. Sci. 63 (2008) 1142–1153.
- [13] S.-Y. Park, C.J. Rutland, K. Narayanaswamy, S.J. Schmiege, Y.-S. He, D.B. Brown, P. I. Mech. Eng. D-J. Aut. 225 (2011) 1641–1659.
- [14] T.C. Watling, M.R. Ravenscroft, G. Avery, Catal. Today 188 (2012) 32–41.
- [15] A. Konstandopoulos, M. Kostoglou, S. Lorentzou, N. Vlachos, Catal. Today 188 (2012) 2–13.
- [16] S.-Y. Park, C. Rutland, Chem. Eng. Sci. 88 (2013) 69–78.
- [17] S.E. Voltz, C.R. Morgan, D. Liederman, S.M. Jacob, Ind. Eng. Chem. Prod. RD 12 (1973) 294–301.
- [18] A.G. Konstandopoulos, J.H. Johnson, SAE Tech. Pap. (1989) 890405.
- [19] A.G. Konstandopoulos, SAE Tech. Pap. (2003), 2003-01-0846.
- [20] G. Croppi, A. Belloli, E. Tronconi, P. Forzatti, Chem. Eng. Sci. 50 (1995) 2705–2715.
- [21] E.J. Bissett, M. Kostoglou, A.G. Konstandopoulos, Chem. Eng. Sci. 84 (2012) 255–265.
- [22] M. Kostoglou, E.J. Bissett, A.G. Konstandopoulos, Ind. Eng. Chem. Res. 51 (2012) 13062–13072.
- [23] VDI-Waermeatlas, Berechnungsunterlagen fuer Druckverlust, Waerme- und Stoffuebergang, 10th ed., Springer, Berlin, 2006.
- [24] E.N. Fuller, P.D. Schettler, J.C. Giddings, J. Ind. Eng. Chem. 58 (1966) 18–27.

- [25] O. Kroeger, M. Elsener, M. Votsmeier, *Ind. Eng. Chem. Res.* 48 (2009) 10746–10750.
- [26] E. Tronconi, P. Forzatti, *AIChE J.* 38 (1992) 201–210.
- [27] W. Hauptmann, M. Votsmeier, H. Vogel, D.G. Vlachos, *Appl. Catal. A* 397 (2011) 174–182.
- [28] A. Scheuer, O. Hirsch, R. Hayes, H. Vogel, M. Votsmeier, *Catal. Today* 175 (2011) 141–146.
- [29] Y. Mizuno, Y. Miyairi, F. Katsume, E. Ohara, A. Takahashi, M. Makino, T. Mizutani, K. Yuki, H. Kurachi, *SAE Tech. Pap.* (2008), 2008-01-0618.
- [30] Y. Furuta, T. Mizutani, Y. Miyairi, K. Yuki, H. Kurachi, *SAE Tech. Pap.* (2009), 2009-01-0292.
- [31] S. Iwasaki, T. Mizutani, Y. Miyairi, K. Yuuki, M. Makino, *SAE Tech. Pap.* (2011), 2011-01-0603.